Phys. Status Solidi B **250,** No. 1, 86–94 (2013) / **DOI** 10.1002/pssb.201248169

physica status solidi b
www.pss-b.com
basic solid state physics

Optoelectronic properties of ABC-stacked trilayer graphene

Y. M. Xiao[1], W. Xu[*,1,2], Y. Y. Zhang[1], and F. M. Peeters[3]

[1] Department of Physics, Yunnan University, Kunming 650091, P. R. China
[2] Key Laboratory of Materials Physics, Institute of Solid State Physics, Chinese Academy of Sciences, Hefei 230031, P. R. China
[3] Department of Physics, University of Antwerp, Groenenborgerlaan 171, B-2020 Antwerpen, Belgium

Received 14 April 2012, revised 3 July 2012, accepted 13 July 2012
Published online 13 August 2012

Keywords ABC stacking, density of states, optical conductance, optoelectronic properties, trilayer graphene

[*] Corresponding author: e-mail wenxu_issp@yahoo.cn, Phone: 86-551-5591335, Fax: 86-551-5594757

We present a theoretical study on the optoelectronic properties of ABC-stacked trilayer graphene (TLG). The optical conductance and light transmittance are evaluated through using the energy-balance equation derived from the Boltzmann equation for an air/graphene/dielectric-wafer system in the presence of linearly polarized radiation field. The results obtained from two band structure models are examined and compared. For short wavelength radiation, the universal optical conductance $\sigma_0 = 3e^2/(4\hbar)$ can be obtained. Importantly, there exists an optical absorption window in the radiation wavelength range 10–200 μm, which is induced by different transition energies required for inter- and intra-band optical absorption channels. As a result, we find that the position and width of this window depend sensitively on temperature and carrier density of the system, especially the lower frequency edge. There is a small characteristic absorption peak at about 82 μm where the largest interband transition states exist in the ABC-stacked TLG model, in contrast to the relatively smooth curves in a simplified model. These theoretical results indicate that TLG has some interesting and important physical properties which can be utilized to realize infrared or THz optoelectronic devices.

1 Introduction Since the historic discovery of isolated graphene in 2004 [1], it has quickly received a great attention in material science, nanoelectronics, and condensed matter physics. Graphene-based material systems are very competitive candidates for advanced electronic and optoelectronic devices due to their excellent electronic, transport, and optical properties along with associated interesting physical features [2]. In graphene, the carrier density can be as high as $10^{13}\,\mathrm{cm}^{-2}$ and can be tuned easily and efficiently by applying the gate voltage [3]. The carrier mobility in graphene can reach up to $20\,\mathrm{m}^2\,\mathrm{V}^{-1}\,\mathrm{s}^{-1}$ at room temperature [4]. As a result, graphene has been proposed as a building block for advanced electronic devices such as graphene p–n and p–n–p junctions [5], high frequency field-effect transistors [6], high frequency electric devices [7], etc. Moreover, graphene has high light transmittance from UV to near-infrared in the air/graphene/dielectric-wafer systems. Therefore, graphene has also been proposed to replace the conventional indium tin oxide (ITO) transparent electrodes [8] in making better and cheaper LED, LCD, infrared photodetectors, etc. At present, the low-cost and reliable growth of high quality and large size graphene films is mainly based on chemical vapor deposition (CVD) technique [9]. Normally the CVD method produces multi-layer graphene films. Hence, the investigation into physical properties of multi-layer graphene systems is of great importance and significance from the view point of device applications.

In order to apply graphene based materials as optoelectronic and transparent electronic devices, the study of its optical and optoelectronic properties is essential. In recent years, the optical and optoelectronic properties of different graphene systems have been investigated intensively. It has been found that the optical conductance per graphene layer is given by a universal value $\sigma_0 = e^2/(4\hbar)$ in the visible bandwidth [10, 11]. The corresponding light transmission coefficients for mono-, bi- and tri-layer graphene on SiO_2 or Si substrates are about 97.7, 95.4, and 93.1%, respectively, and the opacity is about 2.3% per graphene layer [12]. More interestingly, there is an optical absorption window observed experimentally in mono-layer graphene at room-temperature [10, 11] in the mid-infrared to terahertz (THz) regime. We

can reproduce such an optical absorption window for mono- and bi-layer graphene theoretically [13, 14]. Both experimental and theoretical results indicate that the width and depth of this absorption window, especially the lower frequency edge of the window, depend strongly on temperature and carrier density in graphene. This interesting finding implies that graphene systems can be applied for infrared or terahertz (10^{12} Hz or THz) detection in ambient condition.

It is known that multi-layer graphene structures can have an induced energy gap between the conduction and valence bands in the presence of a perpendicular or gate electric field [15–17]. In this regard, trilayer graphene (TLG) is an attractive material system for application in electronic and optoelectronic devices. In contrast to mono- and bi-layer graphene, two stable crystallographic configurations are predicted in TLG: the Bernal stacking (ABA), which has hexagonal symmetry, is common and stable; but some parts of graphite can also have rhombohedral one (the ABC stacking). In a multi-layer graphene system, the stacking order plays an important role in determining its physical properties [18, 19]. At the Dirac point, ABA-stacked TLG is a semi-metal with a gate-tunable band overlap while the ABC-stacked TLG becomes semiconducting with tunable band gaps [18–21]. The existence of the intrinsic small energy gap in ABC-stacked TLG has important implications in band gap engineering for graphene electronics. In conjunction with experimental investigations into the electronic band structure of TLG system, theoretical research in this area has become quite active recently [22, 23, 25–27]. In these theoretical investigations, the effective band structure in the low-energy regime near the *K*-point has been a popularly used model to deal with the electron energy spectrum in ABC-stacked TLG systems [23, 25–27].

The optical and optoelectronic properties of mono- and bi-layer graphene have been studied previously both experimentally and theoretically [8, 10, 12–14]. In contrast to a roughly linear energy spectrum in mono-layer graphene and a parabolic energy spectrum in bi-layer graphene, ABC-stacked TLG has an approximately cubic-like band structure [28]. Thus, the density of states (DoS) for electrons in a ABC-stacked TLG system differs significantly from those in mono- and bi-layer graphene and the corresponding optoelectronic properties may also have different features. In the present study, we intend studying the optoelectronic properties of a gapless ABC-stacked TLG system. We would like to examine the results obtained from popularly used band structure models such as the low-energy effective Hamiltonian model and a simplified model taking from perturbation theory [23, 25].

The paper is organized as follows. In Section 2, we evaluate the optical conductance and transmission coefficient using an energy-balance equation derived from the Boltzmann equation for an air/TLG/dielectric-wafer system in the presence of a linearly polarized radiation field. The results obtained from two model calculations are presented. We also show analytical results for the DoS obtained from two models. The numerical results are presented and discussed in Section 3 and the conclusions drawn from this study are summarized in Section 4.

2 Theoretical approaches

2.1 ABC-stacked trilayer graphene In this study, we consider a system consisting of three layers of graphene sheets in the *xy*-plane on top of a dielectric wafer such as SiO_2 substrate. Including the various interlayer coupling such as the near-neighbor and the next-nearest neighbor interactions, the effective Hamiltonian for a carrier (an electron or a hole) in the ABC-stacked graphene in the π-bands near the *K*-point can be written as [23]

$$H_0 = \begin{pmatrix} R_1 & \hbar^3 v_0^3 k_-^3/\gamma_1^2 + R_2 \\ \hbar^3 v_0^3 k_+^3/\gamma_1^2 + R_2 & R_1 \end{pmatrix}, \tag{1}$$

where $R_1 = \delta - 2v_0 v_4 p^2/\gamma_1$, $R_2 = \gamma_2/2 - 2v_0 v_3 p^2/\gamma_1$, $k_\pm = k_x \pm i k_y = k e^{\pm i\phi}$ with $\boldsymbol{k} = (k_x, k_y)$ being the wavevector for a carrier, $\boldsymbol{p} = \hbar\boldsymbol{k}$ is the momentum operator, and ϕ is the angle between $\boldsymbol{k}$ and the *x*-axis. Moreover, $\gamma_0 = 3.16$ eV, $\gamma_1 = 0.502$ eV, $\gamma_2 = -0.0171$ eV, $\gamma_3 = -0.377$ eV, $\gamma_4 = -0.099$ eV, $\delta = -0.0014$ eV are the Slonczewski–Weiss–McClure (SWM) hopping parameters obtained by fitting the band structures from density-functional theory (DFT) [23] in ABC-stacked TLG. This is a low-energy effective model with $v_i = \sqrt{3}a\gamma_i/2\hbar$ and $a = 2.46$ Å. The corresponding Schödinger equation can be solved analytically and the eigenvalue is given as

$$E_\lambda(\boldsymbol{k}) = h_s + \lambda\sqrt{h_c^2 + h_t^2 + 2\cos(3\phi)h_c h_t}, \tag{2}$$

where $\lambda = +1$ for electron and $\lambda = -1$ for hole, $h_s = \delta - 3\gamma_0\gamma_4(ka)^2/(2\gamma_1)$, $h_c = (\sqrt{3}\gamma_0 ka)^3/(8\gamma_1^2)$, and $h_t = \gamma_2/2 - 3\gamma_0\gamma_3(ka)^2/(2\gamma_1)$. We notice that the energy gap between the conduction and valence bands vanishes at $\cos(3\phi) = 1$ (if h_t is negative) and at $\cos(3\phi) = -1$ (if h_t is positive) [23]. The corresponding eigenfunction for a carrier in ABC-stacked TLG is

$$\psi_{\lambda\boldsymbol{k}}(\boldsymbol{r}) = |\boldsymbol{k}, \lambda\rangle = \frac{1}{\sqrt{2}}[e^{i\psi}, \lambda]\, e^{i\boldsymbol{k}\cdot\boldsymbol{r}}, \tag{3}$$

in the form of a row matrix, with $r = (x, y)$ and $e^{i\psi} = (h_c e^{-3i\phi} + h_t)/B$, $B = \sqrt{h_c^2 + h_t^2 + 2\cos(3\phi)h_c h_t}$.

In the presence of a light field applied perpendicular to the graphene sheet and polarized linearly along the *x*-direction, the carrier–photon interaction Hamiltonian within the usual Coulomb gauge in a ABC-stacked TLG becomes:

$$H'(t) = H'A(t),$$

with

$$H' = \frac{e}{\gamma_1^2}\begin{pmatrix} S_1 & -3\hbar^2 v_0^3 k_-^2 + S_2 \\ -3\hbar^2 v_0^3 k_+^2 + S_2 & S_1 \end{pmatrix}, \tag{4}$$

where $S_1 = 4v_0v_4\hbar k_x\gamma_1$, $S_2 = 4\gamma_1 v_0 v_3 \hbar k_x$, and $A(t) = (F_0/\omega)\sin(\omega t) = (F_0/2i\omega)(e^{i\omega t} - e^{-i\omega t})$ is the vector potential of the radiation field with F_0 and ω being the electric field strength and the frequency of the light field, respectively. The $e^{i\omega t}$ ($e^{-i\omega t}$) term corresponds to the emission (absorption) of a photon. Here we have ignored the contributions from F_0^2 and F_0^3 terms in case of a weak radiation field.

With the electron wavefunction, energy spectrum, and interaction Hamiltonian, one can derive the corresponding electronic transition rate using Fermi's golden rule [24]. In doing so, the first-order contribution to the steady-state electronic transition rate induced by carrier–photon interaction via absorption scattering in TLG is obtained as

$$\begin{aligned} W_{\lambda\lambda'}(\boldsymbol{k},\boldsymbol{k}') &= \frac{2\pi}{\hbar}|\langle\lambda',\boldsymbol{k}'|H'|\boldsymbol{k},\lambda\rangle|^2 \\ &\quad\times\delta[E_{\lambda'}(\boldsymbol{k}') - E_\lambda(\boldsymbol{k}) - \hbar\omega] \\ &= \frac{2\pi}{\hbar}\left(\frac{eF_0}{2\omega}\right)^2\frac{|U_{\lambda\lambda'}(\boldsymbol{k})|^2}{4B^2}\delta_{\boldsymbol{k}',\boldsymbol{k}} \\ &\quad\times\delta[E_{\lambda'}(\boldsymbol{k}') - E_\lambda(\boldsymbol{k}) - \hbar\omega], \end{aligned} \tag{5}$$

which measures the probability for scattering of a carrier from a state $|\boldsymbol{k},\lambda\rangle$ (initial state) to a state $|\boldsymbol{k}',\lambda'\rangle$ (final state) due to absorption of a photon. Here

$$\begin{aligned} |U_{\lambda\lambda'}(\boldsymbol{k})|^2 &= |C[\lambda'(h_c e^{-i\phi} + h_t e^{2i\phi}) + \lambda(h_c e^{i\phi} + h_t e^{-2i\phi})] \\ &\quad + D[\lambda'(h_c e^{-3i\phi} + h_t) + \lambda(h_c e^{3i\phi} + h_t)] \\ &\quad + Q(1+\lambda\lambda')|^2, \end{aligned}$$

with $C = -3\hbar^2 v_0^3 k^2/\gamma_1^2$, $D = 4v_0v_3\hbar k\cos\phi/\gamma_1$, and $Q = 4v_0v_4\hbar Bk\cos\phi/\gamma_1$.

In this work, we use the Boltzmann equation approach to study the response of the carriers in ABC-stacked TLG to the applied radiation field. For a nondegenerate statistics, the semi-classic Boltzmann equation takes a form

$$\frac{\partial f_\lambda(\boldsymbol{k})}{\partial t} = g_s g_v \sum_{\lambda',\boldsymbol{k}'}[F_{\lambda\lambda'}(\boldsymbol{k},\boldsymbol{k}') - F_{\lambda'\lambda}(\boldsymbol{k}',\boldsymbol{k})], \tag{6}$$

where $g_s = 2$ and $g_v = 2$ count for spin and valley degeneracy, respectively, $f_\lambda(\boldsymbol{k})$ is the momentum-distribution function for a carrier at a state $|\boldsymbol{k},\lambda\rangle$, and $F_{\lambda\lambda'}(\boldsymbol{k},\boldsymbol{k}') = f_\lambda(\boldsymbol{k})[1 - f_{\lambda'}(\boldsymbol{k}')]W_{\lambda\lambda'}(\boldsymbol{k},\boldsymbol{k}')$. The Boltzmann equation with the electronic transition rate given above cannot be solved easily and analytically. In the present study, we employ the usual balance-equation approach [13] to approximately solve the problem. For the first moment, the energy-balance equation can be derived by multiplying $\sum_{\boldsymbol{k}} E_\lambda(\boldsymbol{k})$ to both sides of the Boltzmann equation. From the energy-balance equation, we can obtain the energy transfer rate for a carrier: $P_\lambda = \sum_{\boldsymbol{k}} E_\lambda(\boldsymbol{k})\partial f_\lambda(\boldsymbol{k})/\partial t$ and the total energy transfer rate induced by carrier–photon interaction in the system is

$$P = P_{++} + P_{+-} + P_{-+} + P_{--}, \tag{7}$$

with

$$P_{\lambda\lambda'} = 4\hbar\omega\sum_{\boldsymbol{k}',\boldsymbol{k}} F_{\lambda\lambda'}(\boldsymbol{k},\boldsymbol{k}'). \tag{8}$$

With the energy transfer rate P, we can calculate the optical coefficients of the system such as the optical conductance, absorption, and transmission coefficients, etc. The optical conductance $\sigma(\omega)$ can be obtained from $P = \sigma(\omega)F_0^2/2$ and we have

$$\sigma(\omega) = \frac{\sum_{\lambda,\lambda'} P_{\lambda\lambda'}}{F_0^2} = \sum_{\lambda,\lambda'}\sigma_{\lambda\lambda'}(\omega), \tag{9}$$

which does not depend on the radiation intensity F_0 when F_0 is sufficiently weak. We assume that the momentum distribution of a carrier in an ABC-stacked TLG can be described by a statistical energy distribution such as the Fermi–Dirac function $f_\lambda(\boldsymbol{k}) \simeq f_\lambda[E_\lambda(\boldsymbol{k})]$, where $f_\lambda(x) = [1 + e^{(x-\mu_\lambda^*)/k_BT}]^{-1}$ with μ_λ^* being the chemical potential (or Fermi energy at $T \to 0$) for electrons or holes. In the present study, we consider that the radiation field is sufficiently weak so that the electrons in the system are in the linear response regime. In such a situation the effect of electron heating does not occur and, therefore, the electron temperature is the same as the environmental one.

After including the effect of the broadening of the scattering states due to energy relaxation through using the Poisson Kernel to replace the δ function, $\delta(E) \to (E_\tau/\pi)(E^2 + E_\tau^2)^{-1}$, we have

$$\begin{aligned} \sigma_{++}(\omega) &= \frac{2\sigma_0}{3\pi^2\hbar^2\omega^2}\frac{\tau\omega}{(\omega\tau)^2+1} \\ &\quad\times\int_0^\pi d\phi\int_0^\infty\frac{dkk}{B^2}G_{++}(k,\phi) \\ &\quad\times f_+[E_+(\boldsymbol{k})]\{1 - f_+[E_+(\boldsymbol{k})]\}, \end{aligned} \tag{10}$$

for transition within the conduction band, where τ is the energy relaxation time, $E_\tau = \hbar/\tau$ is the energy broadening of the states, $\sigma_0 = 3e^2/(4\hbar)$, and

$$\begin{aligned} G_{++}(k,\phi) &= \left[-\frac{9\sqrt{3}a^3\gamma_0^3k^2}{4\gamma_1^2}(h_c\cos\phi + h_t\cos 2\phi)\right. \\ &\quad + \frac{6a^2\gamma_0\gamma_3 k\cos\phi}{\gamma_1}(h_t + h_c\cos 3\phi) \\ &\quad \left. + \frac{6a^2\gamma_0\gamma_4 kB\cos\phi}{\gamma_1}\right]^2. \end{aligned}$$

For transition within the valance band, we obtain

$$\sigma_{--}(\omega) = \frac{2\sigma_0}{3\pi^2\hbar^2\omega^2}\frac{\omega\tau}{(\omega\tau)^2+1} \times \int_0^{\pi} \mathrm{d}\phi \int_0^{\infty} \frac{\mathrm{d}kk}{B^2} G_{--}(k,\phi) \times f_-[E_-(\boldsymbol{k})]\{1-f_-[E_-(\boldsymbol{k})]\}, \tag{11}$$

with

$$G_{--}(k,\phi) = \left[\frac{9\sqrt{3}a^3\gamma_0^3k^2}{4\gamma_1^2}(h_c\cos\phi + h_t\cos 2\phi) - \frac{6a^2\gamma_0\gamma_3\cos\phi}{\gamma_1}(h_t + h_c\cos 3\phi) + \frac{6a^2\gamma_0\gamma_4 kB\cos\phi}{\gamma_1}\right]^2.$$

For interband transition channels, we have $\sigma_{+-}(\omega) = 0$ and

$$\sigma_{-+}(\omega) = \frac{\sigma_0\tau}{3\pi\hbar^2\omega}\int_0^{\pi}\mathrm{d}\phi\int_0^{\infty}\frac{\mathrm{d}kk}{B^2}\,\mathrm{e}^{-|\tau(\omega-2B/\hbar)|}G_{-+}(k,\phi) \times f_-[E_-(\boldsymbol{k})]\{1-f_+[E_+(\boldsymbol{k})]\}, \tag{12}$$

where we have taken an approximation $\delta(E) \to \mathrm{e}^{-|E|/E_\tau}/(2E_\tau)$ to replace the δ function and

$$G_{-+}(k,\phi) = \left[\frac{9\sqrt{3}a^3\gamma_0^3k^2}{4\gamma_1^2}(h_c\sin\phi - h_t\sin 2\phi) - \frac{6a^2\gamma_0\gamma_3 k\cos\phi}{\gamma_1}h_c\sin 3\phi\right]^2.$$

Using Eqs. (10)–(12) we can evaluate the contributions from different transition channels to the optical conductance in an ABC-stacked TLG.

2.2 A simplified model When considering only the near-neighbor interactions in a TLG, the effective Hamiltonian for a carrier (electron or hole) in the π-bands near the K-point can be simplified as [25]

$$H_0^* = \frac{\hbar^3 v_0^3}{\gamma_1^2}\begin{pmatrix} 0 & k_-^3 \\ k_+^3 & 0\end{pmatrix}, \tag{13}$$

where $\gamma_0 = 3.16\,\mathrm{eV}$, $\gamma_1 = 0.502\,\mathrm{eV}$, $v_0 = \sqrt{3}a\gamma_0/2\hbar$, and $a = 2.46\,\text{Å}$. The corresponding Schödinger equation can be solved analytically. The eigenvalue is obtained as

$$E_\lambda^*(\boldsymbol{k}) = \lambda\frac{(\sqrt{3}\gamma_0 ka)^3}{8\gamma_1^2}, \tag{14}$$

and the corresponding eigenfunction is

$$\psi_{\lambda k}^*(\boldsymbol{r}) = |\boldsymbol{k},\lambda\rangle = \frac{1}{\sqrt{2}}[\mathrm{e}^{-3i\phi},\lambda]\,\mathrm{e}^{i\boldsymbol{k}\cdot\boldsymbol{r}}. \tag{15}$$

When a light radiation field is applied perpendicular to the graphene sheet and is polarized linearly along the x-direction of the graphene system, the carrier–photon interaction Hamiltonian now becomes

$$H'^*(t) = \frac{3\hbar^2 v_0^3 eA(t)}{\gamma_1^2}\begin{pmatrix} 0 & -k_-^2 \\ -k_+^2 & 0\end{pmatrix}. \tag{16}$$

The electronic transition rate induced by carrier–photon interaction via absorption scattering is obtained, from Fermi's golden rule [24], as

$$W_{\lambda\lambda'}^*(\boldsymbol{k},\boldsymbol{k}') = \frac{2\pi}{\hbar}\left(\frac{3\hbar^2 e v_0^3 F_0}{2\gamma_1^2\omega}\right)^2\frac{|U_{\lambda\lambda'}^*(\boldsymbol{k})|^2}{2}\delta_{\boldsymbol{k}',\boldsymbol{k}} \times \delta[E_{\lambda'}^*(\boldsymbol{k}') - E_\lambda^*(\boldsymbol{k}) - \hbar\omega], \tag{17}$$

with $|U_{\lambda\lambda'}^*(\boldsymbol{k})|^2 = k^4[1+\lambda\lambda'\cos(2\phi)]$. After employing the similar energy-balance equation approach as discussed in Section 2.1, the optical conductance induced by different transition channels is given as

$$\sigma_{++}^*(\omega) = \frac{81a^6\gamma_0^6\sigma_0}{16\pi\hbar^2\omega^2\gamma_1^4}\frac{\tau\omega}{(\omega\tau)^2+1}\int_0^{\infty}\mathrm{d}kk^5 f_+[E_+^*(\boldsymbol{k})] \times \{1-f_+[E_+^*(\boldsymbol{k})]\}, \tag{18}$$

$$\sigma_{--}^*(\omega) = \frac{81a^6\gamma_0^6\sigma_0}{16\pi\hbar^2\omega^2\gamma_1^4}\frac{\tau\omega}{(\omega\tau)^2+1}\int_0^{\infty}\mathrm{d}kk^5 f_-[E_-^*(\boldsymbol{k})] \times \{1-f_-[E_-^*(\boldsymbol{k})]\}, \tag{19}$$

and

$$\sigma_{-+}^*(\omega) = \sigma_0 f_-[E_-^*(\boldsymbol{k})]\{1-f_+[E_+^*(\boldsymbol{k})]\}. \tag{20}$$

2.3 Light transmittance The optical transmission coefficient for an air/TLG/dielectric-wafer system can be evaluated through [29]

$$T(\omega) = \sqrt{\frac{\varepsilon_2}{\varepsilon_1}}\frac{4(\varepsilon_1\varepsilon_0)^2}{\left|(\sqrt{\varepsilon_1\varepsilon_2}+\varepsilon_1)\varepsilon_0 + \sqrt{\varepsilon_1}\sigma(\omega)/c\right|^2}, \tag{21}$$

where $\varepsilon_1 = 1$ and $\varepsilon_2 = \varepsilon_\infty$ are the dielectric constant of free space and the effective high-frequency dielectric constant of the substrate, respectively, and c is the speed of light in vacuum. Thus, with the optical conductance $\sigma(\omega)$ we can calculate the light transmittance $T(\omega)$.

2.4 The density of states In order to understand the essential difference of the results obtained from the above-mentioned two theoretical models, it is worth to look into the electronic DoS resulting from the two models for an ABC-stacked TLG. From the electronic energy spectrum, the retarded Green's function for a carrier is $G(E_\lambda) = 1/[E_\lambda - E_\lambda(\boldsymbol{k}) + i\delta]$ with E_λ being the carrier energy. The DoS for electrons in TLG is determined by the imaginary part of the Green's function

$$D(E_\lambda) = \mp g_s g_v \sum_{\boldsymbol{k}} \frac{\mathrm{Im}(E_\lambda)}{\pi} = g_s g_v \sum_{\boldsymbol{k}} \delta[E_\lambda - E_\lambda(\boldsymbol{k})]. \tag{22}$$

For an ABC-stacked TLG, we have

$$D(E_\lambda) = \frac{4}{\pi^2} \int_0^\infty \frac{\mathrm{d}k\, k|E_\lambda - hs|}{\sqrt{4h_c^2 h_h^2 - [(E_\lambda - h_s)^2 - h_c^2 - h_t^2]^2}}, \tag{23}$$

where the integral interval should satisfy the condition: $4h_c^2 h_h^2 - [(E_\lambda - h_s)^2 - h_c^2 - h_t^2]^2 > 0$. For the simplified model for a TLG, we get

$$D^*(E_\lambda) = \frac{8\gamma_1^2}{9\pi\gamma_0^2 a^2 \sqrt[3]{\gamma_1^2 |E_\lambda|}}. \tag{24}$$

3 Results and discussion In Fig. 1, we plot the DoS given by Eqs. (23) and (24) for the ABC-stacked TLG model and the simplified model, respectively, as a function of electron energy E in conduction and valence bands. As we can see, using the ABC-stacked model there are two peaks at the energy $E \sim -8.0$ meV in the valence band and $E \sim 7.0$ meV in the conduction band, respectively. This is caused by the asymmetry of the energy spectrum between conduction and valence bands (see Eq. (23)). Because the DoS obtained from the simplified model is symmetric (see Eq. (24)), the peak of the DoS appears at $E = 0$. Therefore, the DoS in a ABC-stacked TLG model differs significantly from that in the simplified model in the low energy range. Due to the differences of the energy spectra and the corresponding DoS using these two models, one can expect that the optical properties of the TLG would show some different characters by taking these two models.

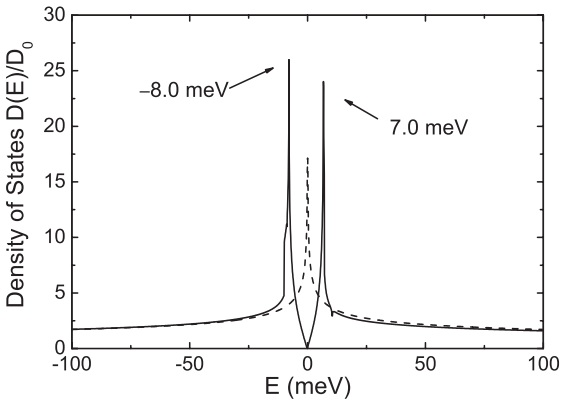

Figure 1 The density of states $D(E)$ for electrons in ABC-stacked TLG as a function of the electron energy E. The results for the ABC-stacked TLG model (solid curve) and for the simplified model (dashed curve) are shown. Here $D_0 = 8\gamma_1^2/(9\pi a^2\gamma_0^2)$.

For numerical calculations, we consider a typical ABC-stacked TLG device in which the conducting carriers are electrons. If n_0 is the electron density in the absence of the radiation field (or dark density), the electron density in the presence of the radiation is $n_e = n_0 + \Delta n_e$, where Δn_e is the density of photoexcited electrons. Under the condition of the charge number conservation $\Delta n_e = n_h$ is the hole density in the presence of radiation field. At a finite temperature, the chemical potential μ_λ^* for electrons and holes in an ABC-stacked TLG can be determined, respectively, through

$$n_e = \frac{2}{\pi^2} \int_0^\pi \mathrm{d}\phi \int_0^\infty \mathrm{d}k\, k f_+[E_+(\boldsymbol{k})] \tag{25}$$

and

$$n_h = \frac{2}{\pi^2} \int_0^\pi \mathrm{d}\phi \int_0^\infty \mathrm{d}k\, k\{1 - f_-[E_-(\boldsymbol{k})]\}. \tag{26}$$

It is known that for an air/graphene/wafer system, the dark electron density can be tuned by, e.g., applying a gate DC voltage. It has been demonstrated theoretically [13] that when the electric component of the radiation field is about $1\,\mathrm{kV\,cm^{-1}}$, the photon-induced carrier density can be generated with about 10% of the dark density in graphene. However, the calculation of photon-excited carrier densities in graphene needs to solve the mass-balance equation (or rate equation) induced by inter-band transition and to include inter-band electron–phonon scattering centers [13]. This complicates the analytical and numerical calculations considerably and we do not attempt it in the present study. In the numerical calculations, we take the electron and hole densities as the input parameters. Moreover, we take $\varepsilon_1 = 1$ and $\varepsilon_2 = 1.5$ for an air/TLG/SiO_2 system, where the effect of the dielectric constant mismatch between TLG and the substrate layer has been taken into account [30]. It has been obtained experimentally [31] that in a graphene device, the energy relaxation time is about $\tau \sim 1$ ps for high-density samples. Thus, we take $\tau \sim 1$ ps in the calculations.

In Fig. 2 we show the contributions from different electronic transition channels to the optical conductance and the corresponding light transmittance for the fixed electron n_e and hole n_h densities at a temperature $T = 150$ K for the ABC-stacked TLG system. We compare the results obtained from an ABC-stacked TLG model (in (a)) and from a simplified model (in (b)). We notice the following features. (i) Inter-band transition from lower-energy valence band to higher-energy conduction band contributes to the optical absorption in the short wavelength regime ($\mathcal{L} < 10\,\mu$m),

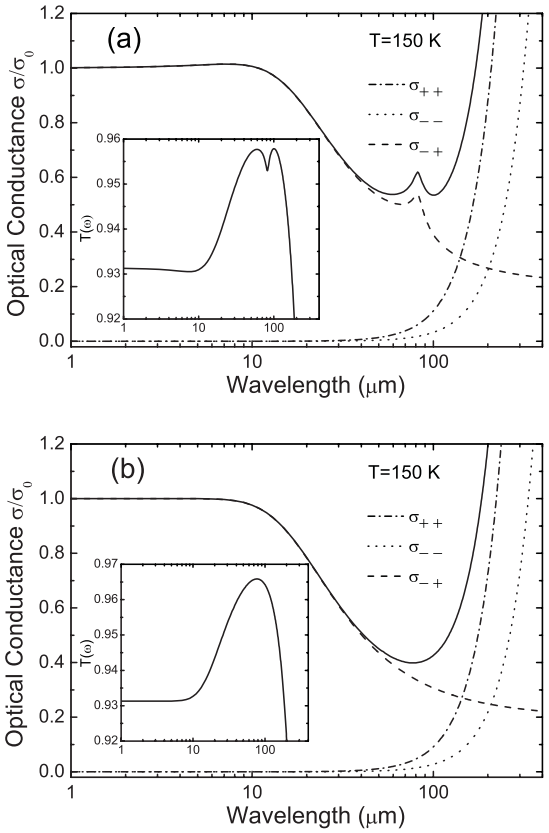

Figure 2 Contributions from different transition channels to optical conductance and the corresponding light transmittance (inset) at $T = 150\,\mathrm{K}$ with carrier densities $n_e = 1.5 \times 10^{12}\,\mathrm{cm}^{-2}$ and $n_h = 5 \times 10^{11}\,\mathrm{cm}^{-2}$. The results obtained from the ABC-stacked TLG model and the simplified model are shown, respectively, in (a) and (b). Here, $\sigma_0 = 3e^2/(4\hbar)$; σ_{++}, σ_{--}, and σ_{-+} are the optical conductance induced by transition within the conduction band, within the valence band and by inter-band transition from valence band to conduction band, respectively. The solid curve is the total optical conductance.

whereas intra-band transitions give rise to the long-wavelength optical absorption. This can be seen from both models. (ii) The optical conductance varies very little with varying the radiation frequency in the short-wavelength regime ($\mathcal{L} < 3\,\mu$m), whereas the optical conductance and transmission coefficient depend strongly on the radiation wavelength in the long-wavelength regime ($\mathcal{L} > 10\,\mu$m). (iii) The optical conductance in the short-wavelength regime is a universal value $\sigma_0 = 3e^2/(4\hbar)$ for ABC-stacked TLG, given by the two models. We note that for mono- and bi-layer graphene the universal optical conductances are $\sigma_0 = e^2/(4\hbar)$ and $\sigma_0 = e^2/(2\hbar)$, respectively. This confirms that the universal optical conductance per graphene layer is $e^2/(4\hbar)$. (iv) In the intermediate radiation wavelength regime ($3 < \mathcal{L} < 50\,\mu$m), the optical conductance increases slightly with radiation wavelength in Fig. 2a while $\sigma(\omega)$ it is almost a straight line in Fig. 2b. (v) More interestingly, there is an absorption window in the 50–500 μm wavelength range, given by both models. A small peak appears at about 82 μm wavelength in Fig. 2a, in contrast to the relatively smooth curve in Fig. 2b. The reason to observe such a small peak can be understood with the help of Fig. 1. The energy difference between the two peaks in Fig. 1a is about 15 meV which corresponds to a wavelength of 82 μm. Thus, the wavelength of 82 μm is at the place where the largest inter-band transition states exist and the small absorption peak shown in Fig. 2a is a consequence of it restricted by the Fermi–Dirac distribution. (vi) The optical absorption window in the simplified model in Fig. 2b has a slight red shift compared to that given by an ABC-stacked TLG model in Fig. 2a.

In general, the optical absorption is induced by the completing electronic transition channels due to inter- and intra-band electronic scattering events. As expected, inter-band transitions require larger photon energies. Intra-band transitions, which are caused by the usual free-carrier absorption, occur under the radiation with lower photon energies. It is a common feature that for free-carrier absorption, the strength of the optical absorption increases rapidly with radiation wavelength. This interesting features can be understood with the help of Fig. 3. When the radiation field is absent, there is a single Fermi level in the conduction band in an n-type ABC-stacked TLG. In this case all states below E_F^e are occupied by electrons, as shown in Fig. 3a. When a light field is applied to the system (see Fig. 3b), the electrons in the valence band are excited into the conduction band via absorption of photons. Thus, the electron density in the conduction band increases and the Fermi level E_F^h is established in the valence band for holes. As shown in Fig. 3b, in the presence of a radiation field the intra-band electronic transition accompanied by the absorption of photons can be achieved not only in the conduction band

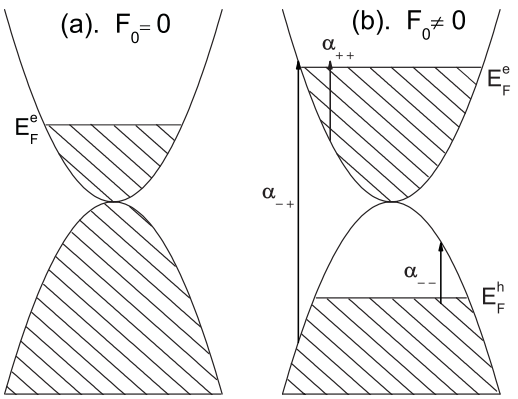

Figure 3 (a) An ABC-stacked TLG system in the absence of the radiation field (i.e., $F_0 = 0$). Here we show the case where the conducting carriers are electrons with a Fermi energy E_F^e in the conduction band. The hatched areas show the occupied states. (b) Optical absorption channels in the presence of a radiation field ($F_0 \neq 0$). Here E_F^e and E_F^h are the quasi-Fermi energies for, respectively, electrons and holes, and there are three optical-absorption channels: α_{-+} for interband transition, α_{++} and α_{--} for intraband transition within the conduction and valence band, respectively.

via a channel α_{++} but also in the valence band via a channel α_{--}. The intra-band transitions are a direct consequence of the broadening of the scattering states in the conduction and valence bands. Because an ABC-stacked TLG is gapless in the absence of a gate-voltage, the electrons in the valence band can be more easily excited into the conduction band in contrast to a conventional semiconductor which has a fundamental band-gap. Thus, there is a strong inter-band optical transition channel, i.e., α_{-+} in Fig. 3b, in an ABC-stacked TLG. Since optical absorption is achieved through electronic transition from occupied states to empty states, the intra-band transitions require less photon energy whereas a relatively large photon energy is needed for inter-band transitions. Consequently, an optical absorption window can be induced through different energy requirements for inter- and intra-band transition channels.

The optical conductance and transmission coefficient obtained from two models are shown in Fig. 4 as a function of radiation wavelength for fixed carrier densities at different temperatures. As can be seen, in the short-wavelength regime $\mathcal{L} < 3\,\mu$m, both σ and $T(\omega)$ depend very little on the radiation wavelength, which can be obtained by using two band structure models. This confirms that σ does not depend on temperature under short wavelength radiation in ABC-stacked TLG. In the long-wavelength regime, in which the optical absorption window can be observed, both the optical conductance and light transmittance depend sensitively on the temperature, in line with experimental findings for monolayer graphene [10]. It should be noted that for fixed electron and hole densities, the chemical potential for electrons/holes decreases/increases with increasing temperature. Thus, due to the Moss–Burstein effect [32], the optical absorption window shifts to the higher energy (or short wavelength) regime with increasing temperature, as shown in Fig. 4. The position of the small absorption peak at about 82 μm wavelength in Fig. 4a does not change with varying temperature and the strength of this peak becomes weaker with increasing temperature. We note that the strength of the optical absorption is proportional to the optical conductance. Therefore, the height of the optical absorption window decreases with increasing temperature. There is a little red shift of the optical absorption window in Fig. 4b compared with that in Fig. 4a at the same temperature. A wider and deeper optical absorption window and a sharper cutoff of the optical absorption at the window edges can be observed at lower temperatures. Such a feature is in line with the temperature dependence of the optical absorption window observed experimentally in monolayer graphene [10, 12].

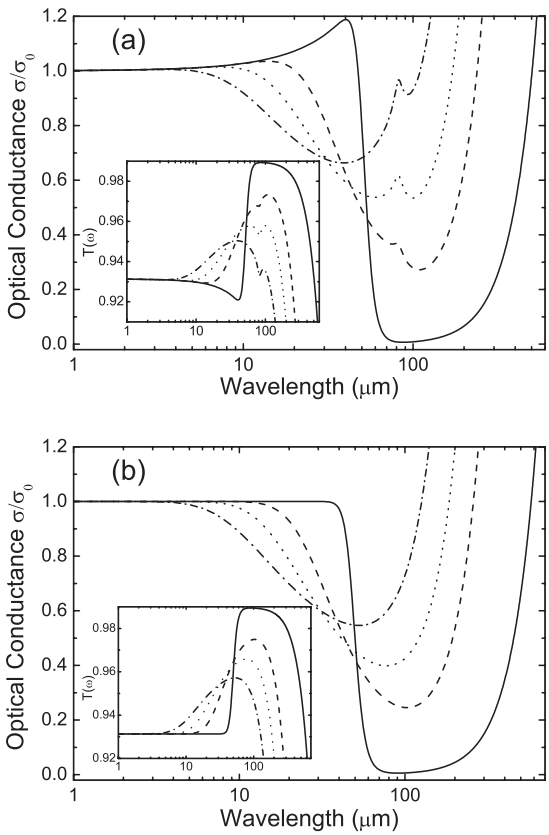

Figure 4 Optical conductance and transmission coefficient (inset) as a function of radiation wavelength at the fixed carrier densities $n_e = 1.5 \times 10^{12}\,\mathrm{cm}^{-2}$ and $n_h = 5 \times 10^{11}\,\mathrm{cm}^{-2}$ for different temperatures $T = 10\,\mathrm{K}$ (solid curve), 77 K (dashed curve), 150 K (dotted curve), and 300 K (dash-dotted curve). The results are shown for (a) the ABC-stacked TLG model and (b) the simplified model.

The optical conductance and transmission coefficient are shown in Fig. 5 as a function of the radiation wavelength at a fixed temperature $T = 150\,\mathrm{K}$ and a fixed hole density n_h for different electron densities n_e. For a gate-controlled TLG placed on a dielectric wafer, the positive (negative) voltage across the gate can pull the electrons (holes) out from the dielectric wafer and inject them into the graphene layer. By doing so, the electron density in the graphene layer can be varied by the gate voltage, and the corresponding optoelectronic properties of the device system depend on the gate voltage applied. This mechanism has been verified experimentally [33]. We see that the optical conductance in the short-wavelength regime depends very little on electron density in a TLG system. Because the chemical potential for electrons in the conduction band increases with electron density, the optical absorption window shifts to the higher energy (or short wavelength) regime with increasing electron density, as shown in Fig. 5. Furthermore, we find that the height of the absorption window increases with electron density and a sharp cutoff of the optical absorption at the window edges can be observed for larger electron density. There is a small red shift of optical absorption window in Fig. 5b compared with that in Fig. 5a at the same electron density. The position of a small absorption peak at about 82 μm depends very little on electron density and the strength of it becomes weaker with increasing electron density. These theoretical results suggest that the width and height of the infrared absorption window in ABC-stacked TLG can be controlled by varying electron density in the system via, e.g., applying a gate voltage.

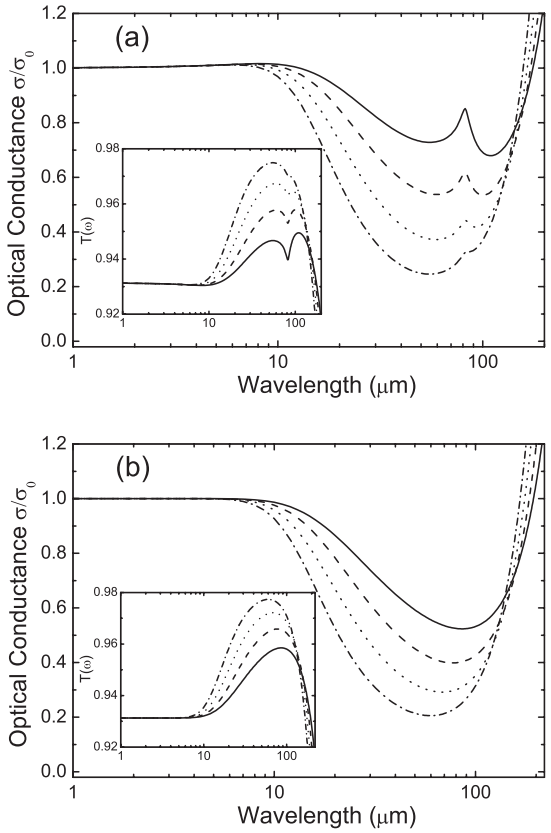

Figure 5 Optical conductance and transmission coefficient (inset) as a function of radiation wavelength at a fixed temperature $T = 150$ K and a fixed hole density $n_h = 5 \times 10^{11}\,cm^{-2}$ for different electron densities $n_e = 1 \times 10^{12}\,cm^{-2}$ (solid curve), $n_e = 1.5 \times 10^{12}\,cm^{-2}$ (dashed curve), $n_e = 2 \times 10^{12}\,cm^{-2}$ (dotted curve), and $n_e = 2.5 \times 10^{12}\,cm^{-2}$ (dash-dotted curve). The results are shown for (a) the ABC-stacked TLG model and (b) the simplified model.

It is known that in an electron gas system, photon-excited carrier densities depend on radiation intensity and temperature. Normally, the photon-induced electron or hole density increases with increasing radiation intensity and/or decreasing temperature. This has been confirmed theoretically for mono-layer graphene based structures [13]. Our previous theoretical results [13] have indicated that the radiation intensity and temperature affect rather significantly the photon-induced carrier densities in graphene. However, when $F_0 < 1\,kV\,cm^{-1}$, the radiation intensity affects relatively weakly the optical conductance or transmittance in graphene, especially in the short-wavelength regime. As we know, varying the radiation intensity and temperature plays a role mainly in varying the quasi Fermi levels of the graphene system. In the short-wavelength regime, because $\hbar\omega \gg E_F^e$ and E_F^h, the optical conductance and transmittance depend very weakly on the radiation intensity and temperature. In the intermediate radiation wavelength regime where the optical absorption window can be observed, one can expect that the optical conductance and transmittance depend relatively strongly on the radiation intensity and temperature. From theoretical results obtained previously [13], we know that when $F_0 < 1\,kV\,cm^{-1}$, a stronger effect of radiation intensity on $\sigma(\omega)$ and $T(\omega)$ in graphene in the window regime can be observed at relatively lower temperatures.

The results shown in Figs. 4 and 5 indicate that the optical conductance and transmittance in TLG in the short wavelength regime depend very little on temperature and electron density. The universal optical conductance for ABC-stacked TLG is $3e^2/(4\hbar)$, in agreement with other theoretical work and experimental findings. In the present study, the coupling of the near-neighbors and the next-nearest neighbors of the graphene layers has been taken into consideration in an ABC-stacked TLG. The simplified model has been taken without inclusion of the coupling of next-nearest neighbors of the graphene layers. Our results show that the main difference obtained from these two models is a small absorption peak at about 82 μm seen in the ABC-stacked TLG model in contrast to a quite smooth curve observed in the simplified model. The optical absorption window has a slight red shift in the simplified model compared to that in the ABC-stacked TLG model. Because the DoS depends weakly on temperature and electron density, the position of the small absorption peak in the ABC-stacked TLG model varies very little with changing temperature and electron density. It should be pointed out further that the value of the optical transmission coefficient shown in Figs. 4 and 5 in the short-wavelength regime agrees quantitatively with that measured experimentally [12]. The strong cutoff of optical absorption at the edges of the optical absorption window can be utilized for the detection of the radiation field, especially for far infrared (FIR) or THz photon detection. We had theoretically studied the optoelectronic properties of mono- and bi-layer graphene [13, 14]. We find that the optical absorption window is red-shifted with increasing number of graphene layers. This interesting feature suggests that the multi-layer graphene based materials can be applied for infrared detections with different detecting bandwidths.

4 Conclusions In this work, we have conducted a detailed theoretical study of the optoelectronic properties of ABC-stacked TLG. On the basis of the semiclassical Boltzmann equation, we have derived the energy-balance equation for an ABC-stacked TLG in the presence of a linearly polarized radiation field. Including intra- and inter-band transition channels, we have studied the dependence of optical absorption/transmission on temperature and electron density in the system. The results obtained from two band structure models have been examined and discussed. The main conclusions drawn from this study are summarized as follows.

In the short-wavelength regime ($\mathcal{L} < 3\,\mu m$), the optical conductance is a universal value $\sigma_0 = 3e^2/4\hbar$ and it depends very little on temperature and electron density. Such an effect can be observed by using both band structure models. This finding confirms that the optical conductance per

graphene layer is given by a universal value $\sigma = e^2/(4\hbar)$ in the short-wavelength regime. The corresponding optical transmission coefficient in this wavelength regime for TLG is about 0.93, in agreement with the experimental data [12].

We have found that there is an optical absorption window in the radiation wavelength range 50–500 μm. Similar to the optical absorption window observed in mono- and bi-layer graphene, the absorption window in TLG is also induced by different transition energies required for inter- and intra-band transition channels. The depth and width of such an absorption window depend sensitively on the temperature and electron density, especially the lower frequency edge. The optical absorption window shows a small red-shift in the simplified model compared to the ABC-stacked TLG model at the same temperature and electron density. There is a small absorption peak at the wavelength about 82 μm in the ABC-stacked TLG model, in contrast to the relatively smooth curve in the simplified model. The position of this small absorption peak does not change with varying temperature and electron density but the strength of it decreases with decreasing temperature and/or increasing electron density. A prominent cutoff of the optical absorption can be observed at the window edges at lower temperature and/or larger electron density. Compared with those obtained from mono- [13], bi- [14], and tri-layer graphene, we find that the optical absorption window red-shifts with increasing number of graphene layers. The results obtained from this study indicate that multi-layer graphene structures, such as TLG, have some interesting and important optoelectronic properties which can be utilized to realize infrared or THz optoelectronic devices.

Acknowledgements This work was supported by the National Natural Science Foundation of China (grant no. 10974206), Department of Science and Technology of Yunnan Province, and by the Chinese Academy of Sciences. One of us (F.M.P.) was a Specially Appointed Foreign Professor of the Chinese Academy of Sciences.

References

[1] K. S. Novoselov, A. K. Geim, S. V. Morozov, D. Jiang, Y. Zhang, S. V. Dubonos, I. V. Grigoreva, and A. A. Firsov, Science **306**, 666 (2004).
[2] S. S. Das, A. K. Geim, P. Kim, and A. H. MacDonald, Solid State Commun. **143**, 1 (2007).
[3] A. K. Geim and K. S. Novoselov, Nature Mater. **6**, 183 (2007).
[4] K. I. Bolotin, K. J. Sikes, J. Hone, H. L. Stormer, and P. Kim, Phys. Rev. Lett. **101**, 096802 (2008).
[5] J. González and E. Perfetto, J. Phys.: Condens. Matter **20**, 145218 (2008).
[6] E. V. Castro, K. S. Novoselov, S. V. Morozov, N. M. R. Peres, J. M. B. Lopes dos Santos, J. Nilsson, F. Guinea, A. K. Geim, and A. H. Castro Neto, Phys. Rev. Lett. **99**, 216802 (2007).
[7] Y.-M. Lin, K. A. Jenkins, A. Valdes-Garcia, J. P. Small, D. B. Farmer, and P. Avouris, Nano Lett. **9**, 422 (2009).
[8] H. Hogan, Photonics Spectra **42**, 19 (2008).
[9] See, e.g., W. Xu, Y. P. Gong, L. W. Liu, H. Qin, and Y. L. Shi, Nanoscale Res. Lett. **6**, 250 (2011).
[10] A. B. Kuzmenko, E. van Heumen, F. Carbone, and D. van der Marel, Phys. Rev. Lett. **100**, 117401 (2008).
[11] Z. Q. Li, E. A. Henriksen, Z. Jiang, Z. Hao, M. C. Martin, P. Kim, H. L. Stormer, and D. N. Basov, Nature Phys. **4**, 532 (2008).
[12] R. R. Nair, P. Blake, A. N. Grigonrenko, K. S. Novoselov, T. J. Booth, T. Stauber, N. M. R. Peres, and A. K. Geim, Science **320**, 1308 (2008).
[13] W. Xu, H. M. Dong, L. L. Li, J. Q. Yao, P. Vasilopoulos, and F. M. Peeters, Phys. Rev. B **82**, 125304 (2010).
[14] H. M. Dong, J. Zhang, F. M. Peeters, and W. Xu, J. Appl. Phys. **106**, 043103 (2009).
[15] Z. Q. Li, E. A. Henriksen, Z. Jiang, Z. Hao, M. C. Martin, P. Kim, H. L. Stormer, and D. N. Basov, Phys. Rev. Lett. **102**, 037403 (2009).
[16] K. F. Mak, C. H. Lui, J. Shan, and T. F. Heinz, Phys. Rev. Lett. **102**, 256405 (2009).
[17] C. H. Lui, Z. Q. Li, K. F. Mak, E. Cappelluti, and T. F. Heinz, Nature Phys. **7**, 944 (2011).
[18] F. Guinea, A. H. Castro Neto, and N. M. R. Peres, Phys. Rev. B **73**, 245426 (2006).
[19] M. Aoki and H. Amawashi, Solid State Commum. **142**, 123 (2007).
[20] W. Bao, L. Jing, Y. Lee, J. Velasco, Jr, P. Kratz, D. Tran, B. Standley, M. Aykol, S. B. Cronin, D. Smirnov, M. Koshin, E. McCann, M. Bockrath, and C. N. Lau, Nature Phys. **7**, 948 (2011).
[21] M. F. Cracium, S. Russo, M. Yamamoto, J. B. Oostinga, A. F. Morpurgo, and S. Tarucha, Nature Nanotechnol. **4**, 383 (2009).
[22] B. Partoens and F. M. Peeters, Phys. Rev. B **74**, 075404 (2006).
A. A. Avetisyan, B. Partoens, and F. M. Peeters, Phys. Rev. B **80**, 195401 (2009).
[23] F. Zhang, B. Sahu, M. Hongki, and A. H. MacDonald, Phys. Rev. B **82**, 035409 (2010).
[24] See, e.g., R. Shankar, Principles of Quantum Mechanics (Plenum Press, New York, 1994), p. 483.
[25] H. Min and A. H. MacDonald, Prog. Theor. Phys. Suppl. **176**, 227 (2008).
[26] S. Yuan, R. Roldán, and M. I. Katsnelson, Phys. Rev. B **84**, 125455 (2011).
[27] M. Koshino and T. Ando, Physica E **40**, 1014 (2008).
[28] M. Koshino and E. McCann, Phys. Rev. B **80**, 165409 (2009).
[29] T. Stauber, N. M. R. Peres, and A. K. Geim, Phys. Rev. B **78**, 085432 (2008).
[30] H. M. Dong, W. Xu, Z. Zeng, T. C. Lu, and F. M. Peeters, Phys. Rev. B **77**, 235402 (2008).
[31] D. Sun, Z.-K. Wu, C. Divin, X. Li, C. Berger, W. A. de Heer, P. N. First, and T. B. Norris, Phys. Rev. Lett. **101**, 157402 (2008).
[32] E. Burstein, Phys. Rev. **93**, 632 (1954).
[33] F. Wang, Y. Zhang, C. Tian, C. Giri, A. Zettl, M. Crommie, and Y. Ron Shen, Science **320**, 206 (2008).

